metals

MDPI

Article

Preparation and Characterization of TiB_2-(Supra-Nano-Dual-Phase) High-Entropy Alloy Cermet by Spark Plasma Sintering

Shulei Zhang, Yuchen Sun, Boren Ke, Yulin Li, Wei Ji *, Weimin Wang and Zhengyi Fu

State Key Laboratory of Advanced Technology for Materials Synthesis and Processing, Wuhan University of Technology, Wuhan 430070, China; zhangshulei@whut.edu.cn (S.Z.); 15370786151231@whut.edu.cn (Y.S.); ke.@whut.edu.cn (B.K.); 1422915370@whut.edu.cn (Y.L.); shswmwang@whut.edu.cn (W.W.); zyfu@whut.edu.cn (Z.F.)

* Correspondence: jiwei@whut.edu.cn; Tel.: +86-027-8786-5484

Received: 29 November 2017; Accepted: 9 January 2018; Published: 17 January 2018

Abstract: This paper introduces the preparation method and characterization results of TiB_2 ceramics with CoCrFeNiAl high-entropy alloy (HEA) as a sintering aid by Spark Plasma Sintering (SPS). Good wettability between HEA and TiB_2 was proved by the sessile drop method, indicating promising prospects for this composite. The sintering results showed that the addition of HEA could dramatically promote the sinterability of TiB_2. TiB_2-5 wt. % HEA dense ceramics prepared at the optimal temperature of 1650 °C showed fine morphology without formation of brittle phases. The liquid phase in the ceramics was highly consistent with the so-called "supra-nano-dual-phase materials (SNDPM)", with near-ideal strength. This study represents the first time that a ceramic-SNDPM composite has been fabricated since the invention of such structures.

Keywords: titanium diboride; high-entropy alloy; cermet; supra-nano-dual-phase

1. Introduction

As an advanced ceramic material, titanium diboride (TiB_2) has been widely applied in many fields, including cutting tools, high-temperature structural components, aluminum evaporation boats, conductive coatings, and armors in the military [1,2] due to its outstanding properties, which include its high melting point (3225 °C), hardness (25–35 GPa), modulus (560 GPa), excellent wear resistance, high chemical stability, and good electrical and thermal conductivity [3,4]. However, because of the oxygen-rich layer (TiO_2 and B_2O_3), strong covalent bonding, and low self-diffusion coefficient, it is difficult to sinter TiB_2 to full density [5,6], even with the assistance of pressure. In order to solve this problem, many methods have been explored. The most common method is to add some nonmetallic or metallic additives. AlN, TiN, Si_3N_4, $TiSi_2$, $MoSi_2$, etc. are generally used as nonmetallic additives [7–10]. However, their effect on lowering the sintering temperature is not obvious. Some transition metallic elements, such as nickel, iron, and titanium have been tested as binders [11–14]. Compared with AlN et al., metals have better wettability with TiB_2. It has been verified by experiments that these metals can dramatically decrease the sintering temperature when sintered with TiB_2 [15]. However, the shortcoming of these metals is also obvious. Secondary borides like M_2B and $M_{23}B_6$ produced during the sintering process greatly embrittle these products. As a result, it is necessary to search for new sintering additives for TiB_2.

The high-entropy alloys (HEAs) designed by Yeh et al. are a new type of material that has been widely discussed in recent years [16]. The alloy contains at least five metallic elements in an equimolar or a near-equimolar ratio from 5 to 35 at. % and the difference of atom radius among all the elements is supposed to be less than 15%. Lattice distortion and sluggish cooperation co-exist in HEA, which

are features of solid-solutions and amorphous phases, respectively; for this reason, HEAs with high mixing entropy of multiple-principal elements cannot be treated as traditional intermetallics. Different metallic element compositions lead to different properties. With proper composition design, the HEA is able to exhibit high hardness and excellent ductility, as well as promising resistances to wear, oxidation and corrosion [6,17]. HEA is an ideal material to act as a new sintering additive [18,19]. Mechanical alloying (MA) is an effective method for synthesizing HEA powder (CoCrFeNiAl, a very classical HEA system) with fine particle size and good chemical uniformity [20]. Therefore, HEA may be used as a sintering additive in ceramics.

In this study, we firstly gained equiatomic CoCrFeNiAl HEA powder by MA. Then, a sessile drop method was used to measure the wettability between as-milled HEA and TiB_2 ceramic. Finally, TiB_2-HEA ceramics were sintered at different temperatures via spark plasma sintering (SPS). In addition, the microstructures and mechanical properties of the bulks were investigated.

2. Materials and Methods

2.1. Powder Preparation

Commercially available titanium diboride powder (purity, 98%; ~3 μm; Hubei Duobo New Ceramic Materials Co., Ltd., Wuhan, China) was used as the raw ceramic. The metal powders supplied by Sinopharm Chemical Reagent Co., Ltd. (Shanghai, China) included cobalt (purity, 99.5%), chromium (purity, 99%), iron (purity, 98%), nickel (purity, 99.9%), and aluminum (purity, 99.5%). The powders were granulated by a 325-mesh sieve.

To mix and mill the metal powders, a high-performance stainless steel vial and stainless steel balls were used as milling agent. The weight ratio of the powders (Co., Cr, Fe, Ni, and Al) to the stainless steel balls was 15:1. The vials were filled with N-heptane to avoid metal oxidation and cold welding. The vials were put in a planetary ball-miller (QM-BP, Nanjing Nanda Instrument Plant, Nanjing, China) for a total milling of 60 h at a speed of 250 rpm in argon atmosphere.

After obtaining the CoCrFeNiAl HEA powders, 95 wt. % TiB_2 and 5 wt. % HEA were mixed with agate balls in polyethylene jars loaded with ethyl alcohol as the medium. The jars were put on a wet ball miller (GMJ/B, Xianyangjinhong General Machinery Co., Ltd., Xianyang, China). After milling for 24 h, the slurry was dried in a rotary evaporator at 65 °C and the obtained powder was subsequently granulated with a 200-mesh sieve.

2.2. Wettability Analysis

High-temperature microscopy (EM-201, Leitz, Stuttgart, Germany) was used to observe the contact angle between TiB_2 and CoCrFeNiAl HEA substrate by sessile drop method [21]. The surface of the TiB_2 substrate was polished, and then sectioned into a wafer with a diameter of 20 mm. The HEA powders were consolidated into the shape of cylinder and positioned in the center of the TiB2 substrate. When the temperature rose from room temperature to 1420 °C (higher than the melting point of the alloy [19]) in the argon atmosphere, the alloy was melted, and the contact angle could be observed.

2.3. Sintering and Characterization

The mixed powders were put in a graphite die with an inner diameter of 20 mm and sintered by SPS (Dr. Sinter-3.20MK II, Sumitomo, Osaka, Japan) at various sintering temperatures (1500 °C, 1550 °C, 1600 °C, 1650 °C and 1700 °C). The other conditions remained the same: a heating rate of 100 °C/min, an axial pressure of 30 MPa, 5 min soaking in vacuum, and free cooling to room temperature after stopping the heating current.

An X-ray diffractometer (XRD, RigakuUltima III, Tokyo, Japan) was used to observe the crystal structure of the as-preserved specimen with Cu Kα radiation, the scanning angle from $2\theta = 10^\circ$ to $2\theta = 90^\circ$, and a scanning rate of 4°/min. Scanning electron microscopy (SEM, Hitachi 3400, Tokyo, Japan) was used to characterize the fracture surfaces of the samples. After ion milling, a thin foil of the

sintered body was observed by transmission electron microscope (TEM, JEOL JEM-2010HT, Tokyo, Japan) equipped with energy-dispersive X-ray spectroscope (EDS, EDAX, Mahwah, NJ, USA) and selected area electron diffraction (SAED). A high-resolution transmission electron microscope (HRTEM, JEOL JEM-2010FEF, Tokyo, Japan) was utilized to obtain more detailed images of the microstructure. The Archimedes' drainage method was used to determine the density of the samples.

2.4. Mechanical Properties

The Vickers hardness was tested with via a Vickers hardness tester (Wolpert-430SV, Wolpert Wilson Instruments, Aachen, Germany) under a load of 5 kg for 15 s. The flexural strength was obtained by three-point bending tests on bars (2 mm × 3 mm × 17 mm) in a ceramic test system (MTS 810, MTS Systems Corporation, Eden Prairie, MN, USA) with a span of 15 mm at a crosshead speed of 0.05 mm/min. Before mechanical testing, the specimens cut from the sintered bulk were polished down to 0.25 μm by diamond suspension and the edges were chamfered in order to eliminate the negative effects of stress concentration. The reported values of all the mechanical properties are the average of 10 measurements.

3. Results and Discussion

Figure 1 shows the XRD patterns of the as-milled powder obtained after various milling times. The XRD patterns of all alloying elements can be observed. After grinding for 6 h, the number of the diffraction peaks was unchanged. After grinding for 18 h, peak broadening occurred and some peaks disappeared. From the XRD patterns, the three most intense peaks can be attributed to the BCC structure ((1 1 0), (2 0 0), (2 1 1)). The BCC phase of CoCrFeNiAl HEA indicated that a simple solid solution was successfully fabricated after milling for 30 h. Further increasing the time above 18 h did not yield any significant difference.

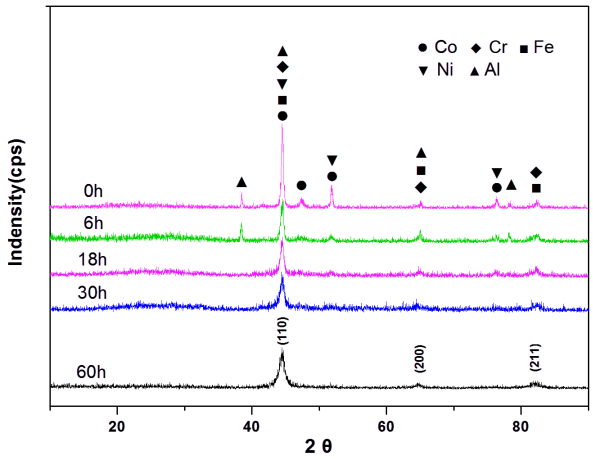

Figure 1. XRD patterns of CoCrFeNiAl HEA during 60 h milling.

Figure 2 shows the results of sessile drop experiments. The contact angles under different temperatures (from 25 °C to 1403 °C) between HEA and the TiB_2 substrate can be seen from these images. Figure 2b reveals that there is no obvious change for either HEA or the ceramic substrate, other than some expansion when the temperature reached 1200 °C. When the temperature rises to 1390 °C, the HEA cylinder starts to melt, and the contact angle between the HEA cylinder and the ceramic substrate can be observed. As shown in Figure 2c–e, when the temperature exceeds 1390 °C, the HEA melts fast, and the contact angle becomes much smaller. Figure 2f indicates that at the end of this process, the molten HEA almost completely spreads onto the substrate. According to the available literature, this result indicates excellent wetting properties between TiB_2 ceramic and

molten CoCrFeNiAl HEA [22]. Wettability is one of the most important aspects for the fabrication of metal-ceramic composites. Good wettability will promote the sinterability of TiB_2 ceramics.

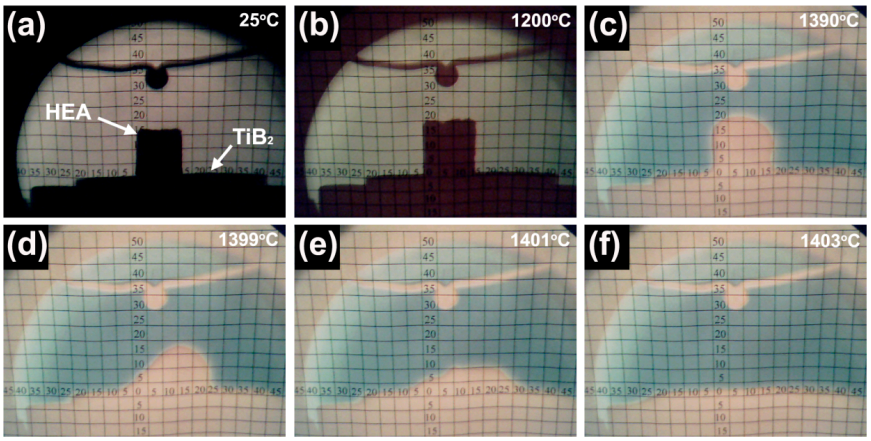

Figure 2. Wetting ability test between CoCrFeNiAl high-entropy alloy and TiB_2 substrate at different temperatures: (**a**) 25 °C; (**b**) 1200 °C; (**c**) 1390 °C; (**d**) 1399 °C; (**e**) 1401 °C and (**f**) 1403 °C.

The XRD patterns of the TiB_2-5 wt. % CoCrFeNiAl mixture and the as-sintered bodies are shown in Figure 3. Only a TiB_2 phase is observed in the mixed powder, and no obvious HEA peak can be observed. The invisibility of the HEA peaks can be ascribed to: Firstly, the MA process causes the low crystallinity of HEA. MA leads to some lattice distortions such as random solid solution, nanoparticles, and the amorphous phase [23]. In addition, HEA only accounts for 5% of the total powders, and cannot be detected. Secondly, both TiB_2 and the as-milled CoCrFeNiAl HEA have peaks at a 2θ of about 44.5°. Therefore, it is difficult to distinguish the HEA peaks from the patterns. As a consequence, XRD, which is used to test the crystalline phase, cannot identify X-ray diffraction peaks whose intensity is not strong enough. Whether the HEA exists or not will be verified in the following discussion. As for the small metallic oxides (MO) phase in the XRD at 1700 °C, the elements with relatively low alloying degrees can exsolute from the HEA and react with the impurities from raw TiB_2 powders to form some metallic oxides. This side reaction is a favorable way of eliminating impurities in raw TiB_2 powder, thus promoting the sinterability of ceramics. Additionally, the peaks of brittle secondary borides (M_2B, $M_{23}B_6$) cannot be observed in the as-sintered ceramics.

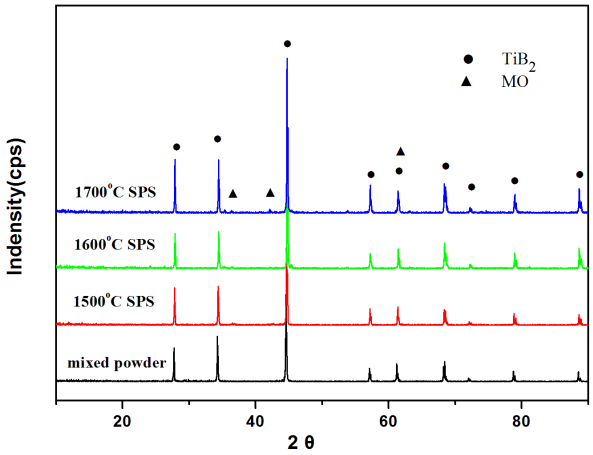

Figure 3. XRD patterns of the mixed powder and TiB_2-5 wt. % HEA ceramics sintered at 1500 °C, 1600 °C, and 1700 °C by SPS.

Figure 4a shows SEM micrographs of the pure TiB_2 ceramic sintered at 1700 °C without a sintering aid. Many open pores exist in the body, and the density is low. Therefore, pure TiB_2 ceramic cannot be easily sintered to high density at temperatures below 1700 °C. SEM micrographs of TiB_2 sintered with 5 wt. % CoCrFeNiAl HEA obtained at different temperatures are shown in Figure 4b–f. The comparison results with/without addition of HEA indicate that the addition of HEA can dramatically promote the sinterability of TiB_2. The relative density of the as-sintered samples with HEA increases with the temperature increase. The few pores observed in Figure 4b indicate that high density cannot be achieved at low temperature (1500 °C). The densification of TiB_2 is remarkably enhanced with the temperature rise, as shown in Figure 4c–f. However, when the temperature reaches 1700 °C, much coarser grains appear. Therefore, 1650 °C is the optimal temperature for obtaining composites with both high density and small grain size, which are the requirements for ceramic materials with good mechanical properties.

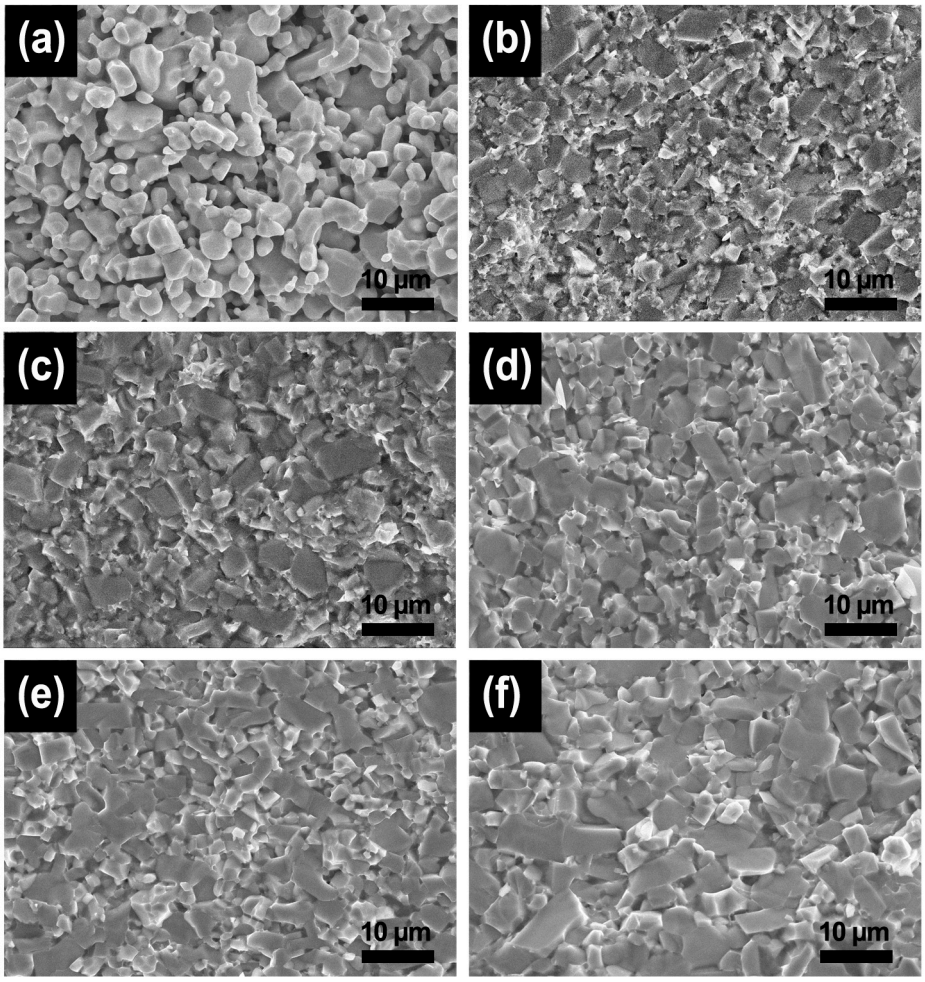

Figure 4. SEM images of (**a**) pure TiB_2 sintered at 1700 °C and (**b**–**f**) TiB_2 with 5 wt. % CoCrFeNiAl high-entropy alloy addition under different temperatures: (**b**) 1500 °C; (**c**) 1550 °C; (**d**) 1600 °C; (**e**) 1650 °C; (**f**) 1700 °C.

High-magnification secondary electron (SE) and backscattered electron (BSE) SEM images of the fracture surface of TiB_2-5 wt. % CoCrFeNiAl ceramics sintered at 1650 °C are shown in Figure 5. The good wettability between TiB_2 and HEA can be certified by the morphology. The bright phase is situated between grain boundaries, and its shape depends on the profile of the adjacent TiB_2 grains. This phase can be preliminarily identified as HEA, because the HEA alloy melts into liquid phases at high temperatures. Liquid phase with excellent fluidity can enhance the densification of ceramics.

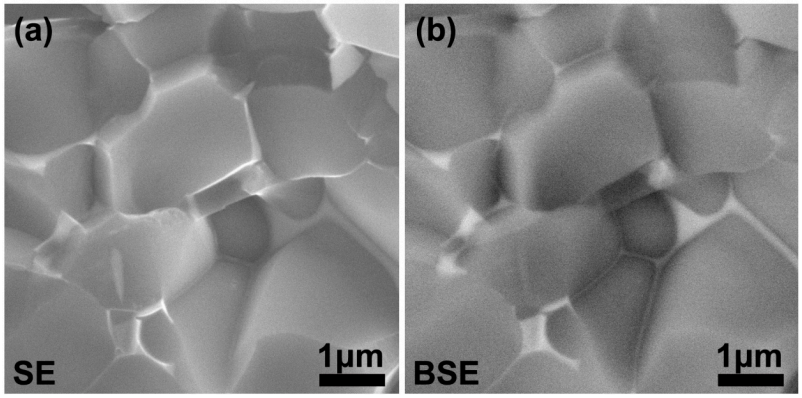

Figure 5. (**a**) SEM SE image and (**b**) the corresponding BSE image of the fracture surface of TiB_2-5 wt. % CoCrFeNiAl composites sintered at 1650 °C.

Figure 6a shows a TEM image of TiB_2-HEA composites sintered at 1650 °C. The corresponding SAED patterns of the sample in Figure 6b reveal that the light area is TiB_2 grain. The EDS result in Figure 6c indicates that the liquid phase surrounded by TiB_2 is HEA, because the elements in this phase only include Cr, Ni, Co., Fe, and Al, which are the original components in the HEA.

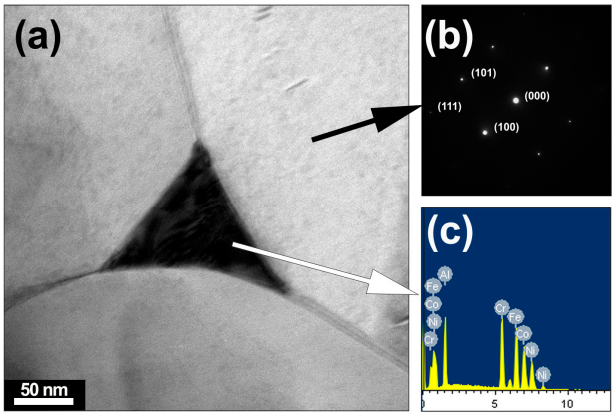

Figure 6. (**a**) TEM images of a bright place selected from the TiB_2-5 wt. % HEA composites sintered at 1650 °C; (**b**) corresponding SAED of grain phase; (**c**) corresponding EDS patterns of liquid phase.

According to the TEM images of the boundary between ceramic and liquid phase in Figure 7a, the lower part is TiB_2, as can be recognized from the complete lattice fringe, whereas the upper part is HEA. The inconspicuous grain boundary between HEA and the ceramics reveals a tight boundary structure, which is favorable to excellent mechanical properties.

HEA phase contains amorphous phases, ordered or disordered solid-solution phases, and nano-sized precipitations. There are two main reasons for the presence of amorphous phases. The first is related to the core effects of HEAs: high entropy effect, severe lattice distortion effect, and sluggish diffusion effect [24]. The high entropy of 1.61 R (R = 8.31 $J \cdot mol^{-1} \cdot K^{-1}$, the gas constant) for CoCrFeNiAl HEA makes it possible to reduce the rate of atomic diffusion and inhibit the crystallization. Secondly, mechanical alloying is in favorable to amorphization. The amorphous phase would be produced during mechanical alloying. According to previous results [24], HEAs containing multiple-principal elements possess sluggish diffusion. The atoms are very hard to replace with others, and the diffusion is inhibited between regions. The diffusion of phase separation is also slow over a long range. All the above factors slow down crystal nucleation and growth, and promote nano-precipitation growth.

For the further confirmation of phase composition, the liquid phase area was observed by HRTEM, as shown in Figure 7b,c. Nanoparticles are conspicuous in the liquid phase of HEA, with a size of 5–10 nm embedded in the amorphous phase. Fast Fourier Transform (FFT) image indicates that these nano-precipitates are simple face-centered cubic (FCC) structures [12]. It is known that the structure of CoCrFeNiAl HEA is body-centered cubic (BCC) following synthesis with the MA process, but the BCC phase prepared in the non-equilibrium process is metastable, and the CoCrFeNiAl HEA will be converted into an FCC structure beyond 1000 °C, according to our previous research [20,25]. Moreover, the particle size is almost the same as that of mechanically alloyed HEAs. Based on the above discussion, the phase composition and distribution are clear. Additionally, the atomic packing rate of FCC structure is 74%, whereas that of BCC structures is only 68%. Dense packing would make the alloy melt with high viscosity and low atomic mobility, which would greatly reduce the nucleation rate and growth velocity, and facilitate amorphization [26,27].

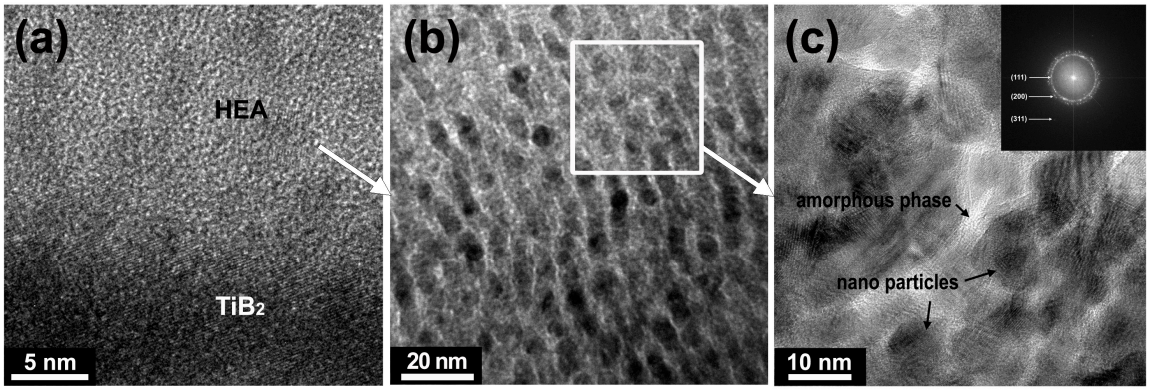

Figure 7. (**a**) HRTEM images of the interface between TiB_2 and HEA for the TiB_2-5 wt. % CoCrFeNiAl HEA composites sintered at 1650 °C; (**b**) Supra-nano-dual-phase structure in the liquid phase and (**c**) HRTEM image of the nanostructured CoCrFeNiAl HEA within amorphous shells. Inset, a fast Fourier transform image of HEA liquid phase.

The combined nanocrystalline-amorphous structure (the size of each phase is less than 10 nm) exhibits near-ideal strength at room temperature [28]. The so-called "supra-nano-dual-phase structure (SNDP)" agrees well with that in the liquid phase in the study. This is the first time a ceramic–SNDP composite has been obtained, and its structure also indicates excellent properties for the TiB_2-HEA cermet.

Figure 8 shows some physical and mechanical properties of TiB_2-5 wt. % HEA ceramics obtained at different sintering temperatures. It is obvious that all the properties increase with the temperature going up from 1500 °C to 1650 °C. The peak values appear at 1650 °C with a relative density of 99.62 ± 0.12%, a flexural strength of 820 ± 9 MPa and a Vickers hardness of 2386 ± 18 HV5. However, when the temperature continues to rise, a slight decreasing trend can be observed in the line chart. The increase in densities and the enhancement of bond strength between TiB_2 and HEA will raise the hardness and strength of the composites. The grain growth caused by high temperatures prevents the further improvement of the mechanical properties.

Barandika reported that monolithic TiB_2 sintered at 1800 °C and 30 MPa showed a relative density of 96.1%, a flexural strength of 367.1 MPa, and a Vickers hardness of 24 GPa [11]. Kang and co-workers obtained 95% densified TiB_2 with Fe addition at a temperature of 2000 °C. The specimen shows a flexural strength of 400 MPa [16]; Park et al. used Si_3N_4 as an additive. The experiment was carried out by hot press sintering at 1800 °C with 30 MPa. The samples provided 97.5% relative density, 500 MPa of flexural strength and 22 GPa of Vickers hardness [10]. To achieve a high relative density (>97%) for monolithic TiB_2 ceramics, a high SPS temperature (>1800 °C) is required [15]. However, in this study, 1650 °C was sufficient to fabricate highly dense ceramics, thus effectively saving energy.

Moreover, compared with other additives, HEA is good for achieving an excellent combination of various mechanical properties, including 99.62% relative density, 820 MPa flexural strength, and 23.89 GPa Vickers hardness. The attractive properties can be attributed to (1) the good wetting ability, which has been proved in wetting ability testing to be conducive to bonding between different phases, and to further enhance mechanical properties; (2) there being no secondary brittle borides (M_2B or $M_{23}B_6$) are produced during sintering; and (3) the excellent mechanical properties of CoCrFeNiAl HEA with a supra-nano-dual-phase structure [29].

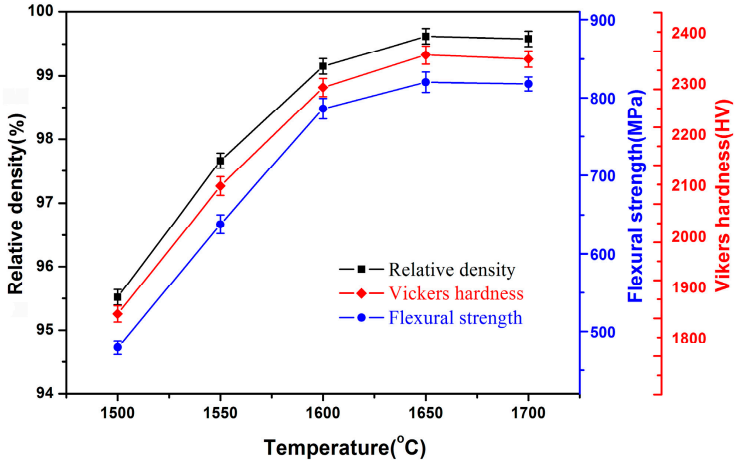

Figure 8. Line chart of mechanical properties of TiB_2-5 wt. % CoCrFeNiAl HEA composites sintered at different temperatures from 1500 °C to 1700 °C.

4. Conclusions

This work mainly focuses on the preparation method and characterization of TiB_2-CoCrFeNiAl high-entropy alloy by spark plasma sintering at different temperatures from 1500 °C to 1700 °C. The conclusions are drawn as follows.

Equiatomic CoCrFeNiAl high-entropy alloy with BCC structure was fabricated by mechanical alloying after 30 h milling.

The HEA spreads on the ceramic substrate completely when the temperature is higher than 1390 °C. The results show excellent wettability between the two phases, which leads to excellent physical compatibility.

The as-sintered TiB_2-HEA bodies do not contain brittle phases, which are expected to degrade the mechanical properties.

TEM images reveal high density and tight grain boundary between TiB_2 ceramic and HEA liquid phase, which are essential requirements for excellent mechanical properties.

The liquid phase in the ceramics agrees well with the so-called "supra-nano-dual-phase materials (SNDPM)" with near-ideal strength.

The TiB_2-HEA composites could be obtained at 1650 °C, which is lower than that obtained in previous studies on TiB_2-based ceramics. Meanwhile, the mechanical and physical properties with a relative density of 99.62 ± 0.12%, a flexural strength of 820 ± 9 MPa and a Vickers hardness of 2386 ± 18 HV5 are superior to previous results.

Acknowledgments: This work was financially supported by the National Natural Science Foundation of China (51521001, 51672197, 5167020705, and 51502220), the National Key Research and Development Plan of China (2017YF130310400), and the Self-determined and Innovative Research Funds of WHUT (2017II17XZ, 2017III03 and 20171049701006). The authors also thank Xuefeng Ruan from School of Power and Mechanical Engineering of Wuhan University for the help in Spark Plasma Sintering, Rong Jiang and Tingting Luo from Materials Analysis Center of Wuhan University of Technology for their help in assisting TEM analyses.

Author Contributions: W.J. and S.Z. conceived and designed the experiments; Y.S. and Y.L. performed the experiments; W.J. and B.K. analyzed the data; W.J. and S.Z. wrote the paper; Z.F. and W.W. modified the paper.

Conflicts of Interest: The authors declare no conflict of interest.

References

1. Wen, G.; Li, S.; Zhang, B.; Guo, Z. Reaction synthesis of TiB_2–TiC composites with enhanced toughness. *Acta Mater.* **2001**, *49*, 1463–1470. [CrossRef]
2. Gu, M.; Huang, C.; Zou, B.; Liu, B. Effect of (Ni, Mo) and TiN on the microstructure and mechanical properties of TiB_2 ceramic tool materials. *Mater. Sci. Eng. A* **2006**, *433*, 39–44. [CrossRef]
3. Basu, B.; Raju, G.B.; Suri, A.K. Processing and properties of monolithic TiB_2 based materials. *Int. Mater. Rev.* **2006**, *51*, 352–374. [CrossRef]
4. Vallauri, D.; Adrian, I.C.A.; Chrysanthou, A. TiC-TiB_2 composites: A review of phase relationships, processing and properties. *J. Eur. Ceram. Soc.* **2008**, *28*, 1697–1713. [CrossRef]
5. Raju, G.; Mukhopadhyay, A.; Biswas, K.; Basu, B. Densification and high-temperature mechanical properties of hot pressed TiB_2–(0–10 wt.%) $MoSi_2$composites. *Scr. Mater.* **2009**, *61*, 674–677. [CrossRef]
6. Wang, W.; Fu, Z.; Wang, H.; Yuan, R. Influence of hot pressing sintering tempera-ture and time on microstructure and mechanical properties of TiB_2 ceramics. *J. Eur. Ceram. Soc.* **2002**, *22*, 1045–1049. [CrossRef]
7. Li, L.; Kim, H.; Kang, E. Sintering and mechanical properties of titanium diboride with aluminum nitride as a sintering aid. *J. Eur. Ceram. Soc.* **2002**, *22*, 973–977. [CrossRef]
8. Park, J.; Koh, Y.; Kim, H.; Hwang, C.; Kang, E. Densification and mechanical properties of titanium diboride with silicon nitride as a sintering aid. *J. Am. Ceram. Soc.* **1999**, *82*, 3037–3042. [CrossRef]
9. Mukhopadhyay, A.; Raju, G.; Basu, B.; Suri, A. Correlation between phase evolution, mechanical properties and instrumented indentation response of TiB_2-based ceramics. *J. Eur. Ceram. Soc.* **2009**, *29*, 505–516. [CrossRef]
10. Zheng, L.; Li, F.; Zhou, Y. Preparation, microstructure, and mechanical properties of TiB_2 using Ti_3AlC_2 as a sintering aid. *J. Am. Ceram. Soc.* **2012**, *95*, 2028–2034. [CrossRef]
11. Barandika, M.; Sanchez, J.; Rojo, T.; Cortes, R.; Castro, F. Fe-Ni-Ti binder phases for TiB_2-based cermets: A thermodynamic approach. *Scr. Mater.* **1998**, *39*, 1395–1400. [CrossRef]
12. Einarsrud, M.; Hagen, E.; Pettersen, G.; Grande, T. Pressureless sintering of titanium diboride with nickel, nickel boride and iron additives. *J. Am. Ceram. Soc.* **1997**, *8*, 3013–3020. [CrossRef]
13. Zhang, Z.; Shen, X.; Wang, F.; Lee, S.; Fan, Q.; Cao, M. Low-temperature densification of TiB_2 ceramic by the spark plasma sintering process with Ti as a sintering aid. *Scr. Mater.* **2012**, *66*, 167–170. [CrossRef]
14. Kang, E.; Jang, C.; Lee, C.; Kim, C.; Kim, D. Effect of iron and boron carbide onthe densification and mechanical properties of titanium diboride ceramics. *J. Am. Ceram. Soc.* **1989**, *72*, 1868–1872. [CrossRef]
15. Zhang, J.; Fu, Z.; Wang, W.; Wang, H.; Min, X. Wettability between TiB_2 ceramic and metals. *Acta Metall. Sin.* **1999**, *12*, 395–400.
16. Yeh, J.-W.; Chen, S.-K.; Lin, S.-J.; Gan, J.-Y.; Chin, T.-S.; Shun, T.-T.; Tsau, C.-H.; Chang, S.-Y. Nanostructured high-entropy alloys with multiple principal elements: Novel alloy design concepts and outcomes. *Adv. Eng. Mater.* **2004**, *6*, 299–303. [CrossRef]
17. Otto, F.; Yang, Y.; Bei, H.; George, E. Relative effects of enthalpy and entropy on the phase stability of equiatomic high-entropy alloys. *Acta Mater.* **2013**, *61*, 2628–2638. [CrossRef]
18. Zhu, G.; Liu, Y.; Ye, J. Fabrication and properties of Ti(C, N)-based cermets with multi-component AlCoCrFeNi high-entropy alloys binder. *Mater. Lett.* **2013**, *113*, 80–82. [CrossRef]
19. Fu, Z.; Koc, R. Processing and characterization of TiB_2-TiNiFeCrCoAl high-entropy alloy composite. *J. Am. Ceram. Soc.* **2017**, *100*, 2803–2813. [CrossRef]
20. Ji, W.; Fu, Z.; Wang, W.; Wang, H.; Zhang, J.; Wang, Y.; Zhang, F. Mechanical alloying synthesis and spark plasma sintering consolidation of CoCrFeNiAl high-entropy alloy. *J. Alloys Compd.* **2014**, *589*, 61–66. [CrossRef]
21. Zheng, X.; Shen, P.; Han, X.; Lin, Q.; Qiu, F.; Zhang, Y.; Jiang, Q. Wettability and reactivity between B_4C and Molten $Zr_{55}Cu_{30}Al_{10}Ni_5$ metallic glass alloy. *Mater. Chem. Phys.* **2009**, *117*, 377–383. [CrossRef]

22. Aizenshtein, M.; Froumin, N.; Frage, N. The nature of TiB_2 wetting by Cu and Au. *J. Mater. Eng. Perform* **2012**, *21*, 655–659. [CrossRef]
23. Varalakshmi, S.; Kamaraj, M.; Murty, B. Synthesis and characterization of nanocrystalline AlFeTiCrZnCu high entropy solid solution by mechanical alloying. *J. Alloys Compd.* **2008**, *460*, 253–257. [CrossRef]
24. Zhang, X.; Zhang, Y.; Qiao, Y.; Chen, G. Novel microstructure and properties of multicomponent $CoCrCuFeNiTi_x$ alloys. *Intermetallics* **2007**, *15*, 357–362. [CrossRef]
25. Ji, W.; Wang, W.; Wang, H.; Zhang, J.; Wang, Y.; Zhang, F.; Fu, Z. Alloying behavior and novel properties of CoCrFeNiMn high-entropy alloy fabricated by mechanical alloying and spark plasma sintering. *Intermetallics* **2015**, *56*, 2–27. [CrossRef]
26. Li, Y.; Guo, Q.; Kalb, J.A.; Thompson, C.V. Matching glass-forming ability with the density of the amorphous phase. *Science* **2008**, *322*, 1816–1819. [CrossRef] [PubMed]
27. Li, R.; Pang, S.; Men, H.; Ma, C.; Zhang, T. Formation and mechanical propertie sof (Ce-La-Pr-Nd)-Co-Al bulk glassy alloys with superior glass-forming ability. *Scr. Mater.* **2006**, *54*, 1123–1126. [CrossRef]
28. Wu, G.; Chan, K.; Zhu, L.; Sun, L.; Lu, J. Dual-phase nanostructuring as a route to high-strength magnesium alloys. *Nature* **2017**, *545*, 80–83. [CrossRef] [PubMed]
29. Zhang, Y.; Zuo, T.T.; Tang, Z.; Gao, M.C.; Dahmen, K.A.; Liaw, P.K.; Lu, Z.P. Microstructures and properties of high-entropy alloys. *Prog. Mater. Sci.* **2014**, *61*, 1–93. [CrossRef]